ISSN 1069-3513, Izvestiya, Physics of the Solid Earth, 2010, Vol. 46, No. 8, pp. 679–697. © Pleiades Publishing, Ltd., 2010.
Original Russian Text © M.N. Berdichevskii, E.Yu. Sokolova, Iv.M. Varentsov, A.K. Rybin, N.V. Baglaenko, V.Yu. Batalev, N.S. Golubtsova, V.E. Matyukov, P.Yu. Pushkarev, 2010, published in Fizika Zemli, 2010, No. 8, pp. 36–53.

Geoelectric Section of the Central Tien Shan: Analysis of Magnetotelluric and Magnetovariational Responses along the Naryn Geotraverse

M. N. Berdichevsky[a†], E. Yu. Sokolova[b], Iv. M. Varentsov[b], A. K. Rybin[c], N. V. Baglaenko[b], V. Yu. Batalev[c], N. S. Golubtsova[a], V. E. Matyukov[c], and P. Yu. Pushkarev[a]

[a] *Geological Faculty, Moscow State University, Moscow, 119991 Russia*

[b] *Geoelectromagnetic Research Centre, Schmidt Institute of Physics of the Earth (IPE), Russian Academy of Sciences, Troitsk, Moscow oblast, 142092 Russia*

[c] *Research Station Bishkek, Kyrgyzstan*

e-mail: sokol_1@mail.ru

Received January 25, 2010

Abstract—During the past two decades, at the Research station (Bishkek) more than a hundred magnetotelluric and magnetovariational soundings were carried out on the Naryn geotraverse that intersects the Tien Shan region from Lake Balkhash to the Tarim Basin along the 76° E meridian. Integration and complex interpretation of the data of these soundings with improved resolution and reliability of the geoelectric model of the Central Tien Shan section became an urgent challenge. Our paper presents a complex of methods for processing and invariant analysis of the electromagnetic data developed for the solution of this problem. Its application allowed us to validate the choice of the 2D interpretation model for the Naryn Line and to form the adequate ensemble of the data to be inverted. The developed approaches will also be useful in similar studies in the other mountain regions.

DOI: 10.1134/S1069351310080057

INTRODUCTION

The Tien Shan region is a unique object for studying the geodynamical processes of the present-day intracontinental orogeny. Here, under the guidance of the Research station in Bishkek, complex geological-geophysical studies of the fundamental problems of geodynamics have been intensively conducted during the past twenty years [*Contemporary geodynamics...*, 2005]. The methods of deep geoelectrics, primarily, the magnetotelluric (MT) and magnetovariational (MV) methods, are essential elements of this complex and make an important contribution to understanding the tectonic structure, fluid, and thermal conditions of the Earth's interiors.

The first systematic ideas concerning the geoelectric structure of the Earth's crust of the region were obtained from the data of MT/MV soundings carried out using the exploration instrumentation in the 1980s and 1990s on a series of geotraverses intersecting the Tien Shan [Trapeznikov et al., 1997; Rybin, 2001]. The history of these works, carried out in collaboration with the scientists of Moscow State University, is presented in the paper [Berdichevsky et al., 2010].

The Naryn geotraverse, which is the most representative one in this series in terms of its extension and the number of soundings, passes along the 76°E meridian through the Central Tien Shan where the geodynamic activity of the entire orogen is focused. For obtaining more adequate information about the deep distribution of the electrical conductivity, 19 long-period soundings were carried out there in 1999–2000 [Bielinski et al., 2003]. Then, in 2005 and 2007 detailed soundings with the new-generation exploring instrumentation were conducted in the revealed regions with the most complex structure. The combined set of soundings on the Naryn Line is presented in Fig. 1. It is important to emphasize that at most points of this set not only MT, but also MV, soundings were carried out. Moreover, since the late 1990s, nearly all soundings were conducted simultaneously by several stations.

Pooling the unique (as to the density and the interval of periods), although very different data sets on this profile and conducting their joint interpretation aimed at the construction of the reference geoelectric section of the Central Tien Shan with up-to-date resolution and reliability was an actual issue. The development of a reasonable complex of methods suitable for solving this problem became the main research trend in the activity of the NARYN Working Group, which included scientists from the Research station in Bishkek, Moscow State University, and the Geoelectromagnetic Research Centre, Schmidt Institute of Phys-

† Deceased.

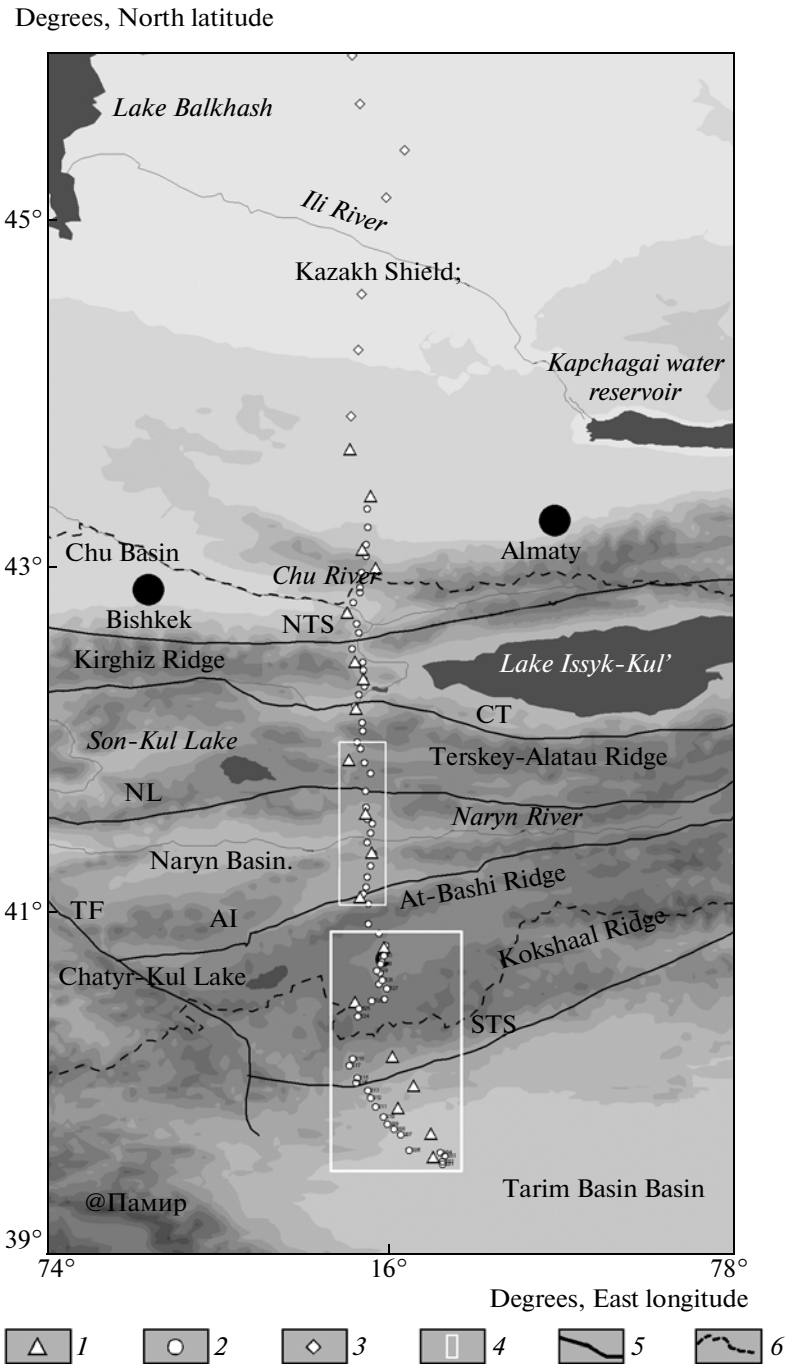

Fig. 1. Layout diagram of the location of the observation points of the MT/MV soundings along the Naryn geotraverse against the background of the topographic map of the Central Tien Shan and adjacent territories: (*1*) the observation points of the LIMS long-period soundings, (*2*) the observation points of the CES-2 soundings, (*3*) the observation points of the MT-PIK soundings, (*4*) the regions of the detailed Phoenix soundings, (*5*) the main faults (the North Tien Shan (NTS), the Central Terskey (CT), the Nikolaev Line (NL), the Atbashi–Inylchek (AI), the Talas–Fergana (TF), and the South Tien Shan (STS)), (*6*) the border of Kyrgyzstan.

ics of the Earth (IPE), Russian Academy of Sciences, in Troitsk, the authors of this paper. Our task was to develop the algorithms for processing, analysis, and two-dimensional (2D) interpretation of the complex of MT and MV data taking into account the specificity of the soundings groups and specific features of the region. The accent in this work was made on the most complete use of the resources of simultaneity of

soundings, on obtaining deep electromagnetic (EM) responses free from the distorting influence of the near-surface structures, on the application of multicomponent 2D inversion taking into account the topography and three-dimensionality of several elements of the data to be interpreted.

The obtained results improved the quality of the data and the efficiency of the solution of the interpretation problems in the complex quasi-2D media compared to our previous works [Varentsov et al., 1996; Vanyan et al., 1998; 2002; Berdichevsky et al., 2003; Rybin, 2001; Bielinski et al., 2003].

The results obtained by the NARYN Working Group, including the developed methodic approaches, which are also useful for the analysis of electromagnetic responses in the other mountain regions, will be presented in a series of concluding publications. In the present paper, which is the first in this series, we summarize the results obtained at the initial stage of the development of interpretation model and describe the results of verification and analysis of MT and MV responses presented, obtained from the entire set of soundings on the Naryn Line. The possibility for their interpretation in the context of the 2D approach is analyzed and validated. We present the multicomponent ensemble of the MT/MV transfer operators (the impedance, the tipper, and the horizontal MV response) estimated in the composite interval of periods from 0.1 s to16 384 s, which is subject to further interpretation.

We also consider important methodic results, including, primarily, the new schemes for the multipoint noise–suppression assessment of the local transfer operators (the impedance $\mathbf{Z}$ and the tipper $\mathbf{W}_z$) and the two-point synchronous horizontal MV operator $\mathbf{M}$. We describe the new methods for the invariant analysis of the transfer operators aimed at the determination of the dimensionality of the geoelectric medium and the strike of the prevailing deep structures in the presence of near-surface galvanic distortions.

The subsequent papers will address the two complementary approaches to the inversion of the constructed data, which are being simultaneously developed by the NARYN group and based on the different modifications of the general algorithm of the inverse problem solution proposed in the works [Varentsov, 2002; 2007]. The first approach [Berdichevsky et al., 2010] invokes only the long-period data for a maximally stable construction of a relatively simple geoelectric model along the Naryn profile. The strategy [Berdichevsky et al., 2003] of successive partial inversions of this data is applied, and the priority is given to the MV responses (tippers) and the impedance phases. The second approach is based on a substantially more detailed piecewise-continuous parameterization of the model; in this approach, the schemes of weighed multicomponent inversion are applied in order to extract the most complete information from the pooled data set comprising the prospecting and the long-period intervals. The preliminary results of this approach appear promising [Sokolova et al., 2005; 2007; 2008].

1. MT/MV SOUNDINGS ON THE NARYN PROFILE

The basis for the heterogeneous grid of EM observations at the Naryn profile (Fig. 1) was laid by 42 local soundings at periods from 0.1 to 1600 s, measured, using the CES-2 (the Kyrgyz Tien Shan) and MT-PIK (the Kazakh Plate) stations, by the staff of the Research station in the 1980s and the 1990s [Trapeznikov et al., 1997].

The progress in the deep Earth studies was ensured by the five-component soundings with the Canadian long-period LIMS stations, carried out in 1999–2000 simultaneously in groups of 5, 10, and 4 observation points in the southern (the Northern Tarim), the central (the Kyrgyz Tien Shan), and the northern (the Kazakh Plate) segments of the profile, respectively. The 20-day-long LIMS observations with a sampling interval of 2 s were supplemented at each observation point by the local prospecting soundings with the American MT24 (EMI) instrumentation, which ensured the composite interval of sounding periods from 0.003 to 16384 s. These soundings were carried out by the team of the Research station together with American geophysicists from the University of California, Riverside [Rybin et al., 2001; Bielinski et al., 2003]. The geoelectric model constructed by them reveals appreciable variations in the electrical conductivity in the Earth's crust and the upper mantle along the profile. A region with the most complex geoelectric structure was identified within the Naryn basin, framed on the north by the most important structural feature of the region, namely, Nikolaev Line fault zone that divides the Caledonides of the North Tien Shan and Caledonian–Hercynian structures of the Central Tien Shan.

For detailed exploration of the Naryn region, in 2005, 23 wide-range (0.003–2048 s) pairwise-synchronous soundings were carried out using the Canadian Phoenix prospecting stations. In 2007, 18 similar soundings with Phoenix instrumentation were executed on the MANAS seismic line adjacent to the southern end of the Naryn profile [Rybin et al., 2008]. These measurements ensured sufficient resolution of studying the junction zone between the Tarim and the South Tien Shan.

2. NEW PROCESSING RESULTS OF THE SYNCHRONOUS SOUNDINGS AND THE RESULTANT SET OF MT/MV RESPONSES

The synchronous electromagnetic soundings with the natural field excitation became presently the most important tool for studying the geoelectric structure of

the lithosphere [Berdichevsky and Zhdanov, 1981; Egbert, 2002; Varentsov, 2007b], since they ensure efficient suppression of the local electromagnetic noise [Gamble et al., 1979; Varentsov et al., 2003; Sokolova and Varentsov, 2005; Ernst et al., 2008] as well as the distortions, caused by the heterogeneous structure of the field excitation [Varentsov and Sokolova, 2003], and supplement the set of the interpretation data by the new synchronous responses [Varentsov, 2005]. The Central Tien Shan became one of the main research areas for development and testing the methods and techniques of synchronous EM sounding.

The Procedure of Synchronous Data Processing

For the advanced processing of synchronous observations on the Naryn profile (the 1999–2000 LIMS data and the 2005–2007 Phoenix data), the multisiteprocedures of evaluation of transfer operators were applied: the mRR (the multi remote reference) method, [Varentsov et al., 2003] based on the robust averaging of RR-estimates (remote reference estimates) for several reference observation points, and its new modification, the mRRMC (the multi remote reference with magnetic control) method [Varentsov and Sokolova, 2005; Varentsov, 2007b]. The mRRMC procedure imposes the constraints on the variations of the horizontal MV responses between the sounding point and the remote bases when selecting the segments of the synchronous multipoint records of the EM field for processing, thereby focusing the evaluation of transfer operators on the data which best meet the criteria of uniform external field and a limited EM noise.

Using the new methods we succeeded in increasing the stability of the evaluation of local transfer operators $\mathbf{Z}$ and $\mathbf{W}_z$ for the LIMS data compared to the results of preprocessing [Rybin et al., 2001], carried out in accordance with the Chave program [Chave et al., 1987]. The most noticeable increase in accuracy is achieved for the additional impedance components (Fig. 2a), which made it possible to further increase the determination accuracy of its invariant parameters that generally depend on all four scalar elements of the impedance tensor. The reliable long-period (above 10000 s) estimates provided by mRRMC averaging expanded the resolving possibilities for the upper-mantle geoelectric structures. Unfortunately, the LIMS data at only 14 observation points in Kyrgyzstan and Kazakhstan were processed using the new procedure. The time series for five Chinese soundings (points 601–605) were unavailable, and in the further analysis of these time series we had to confine ourselves to not quite stable at long periods (especially in the additional impedances) estimates of $\mathbf{Z}$ and $\mathbf{W}_z$, carried out with the use of the Chave program.

The present study on the Naryn profile yielded for the first time reliable estimates for the horizontal MV operator $\mathbf{M}$ (a transfer operator linking the horizontal magnetic fields at the sounding point and at the reference point) in the Central Tien Shan. These synchronous MV responses are important interpretation resources [Varentsov and EMTESZ-Pomerania WG, 2005; Varentsov, 2007b]. Initially, the horizontal MV responses for the subsets of Kyrgyz and Kazakh LIMS observation points were determined relative to points 410 and 411, respectively. The obtained results, which are stable at periods from 16 to 32 768 s, were reduced to a common base at point 410 with the aid of the additional synchronous observations in 2005 at these reference observation points.

The data of 23 MT soundings executed in 2005 with the Phoenix instrumentation for detailed studying of the segment of the profile in the region of the Nikolaev Line fault zone were processed using the RRMC method with the control of the horizontal magnetic links at the pairwise-synchronous observation points. A large portion of the territory of Kyrgyzia is characterized by low industrial electromagnetic noise; at the same time, the severe conditions of the electric lines' grounding in mountains, enhanced uncertainties in the orientation of the induction magnetic sensors (especially the vertical sensor), and the strong wind noise in some cases noticeably impair the quality of the obtained results. The noise-suppressing RRMC technology applied in the construction of estimates of $\mathbf{Z}$ and $\mathbf{W}_z$ facilitated the stabilization of the results in the interval of low-energy variations of the EM field (0.1–10 s). The use of the standard technique of the day-long Phoenix observations using low-frequency instrument filters hampered obtaining reliable results at periods exceeding 1000 s. In a number of cases it was possible to attain the stabilization of the results at periods 1000–2000 s by using the second base (the stationary observation point at the research area of the Bishkek Scientific Station at a distance of more than 300 km).

The Composite Ensembles of the Transfer Operators

The results of advanced processing of LIMS and Phoenix soundings were integrated with the reliable estimates of $\mathbf{Z}$ and $\mathbf{W}_z$ obtained earlier from the CES-2, MT-PIK and MT24 data, and also with the standard Phoenix estimates for soundings carried out in 2007 on the MANAS geotraverse [Rybin et al., 2008]. For the Phoenix soundings located near the LIMS or CES-2 observation points, the comparison of all available results was conducted and, based on the consistent data, averaged broadband estimates were constructed (Fig. 2b). Thus the multicomponent set of the single-site (local) and two-site (synchronous) values of the EM field transfer operators in the composite interval of periods from 0.003 to 16384 s was formed

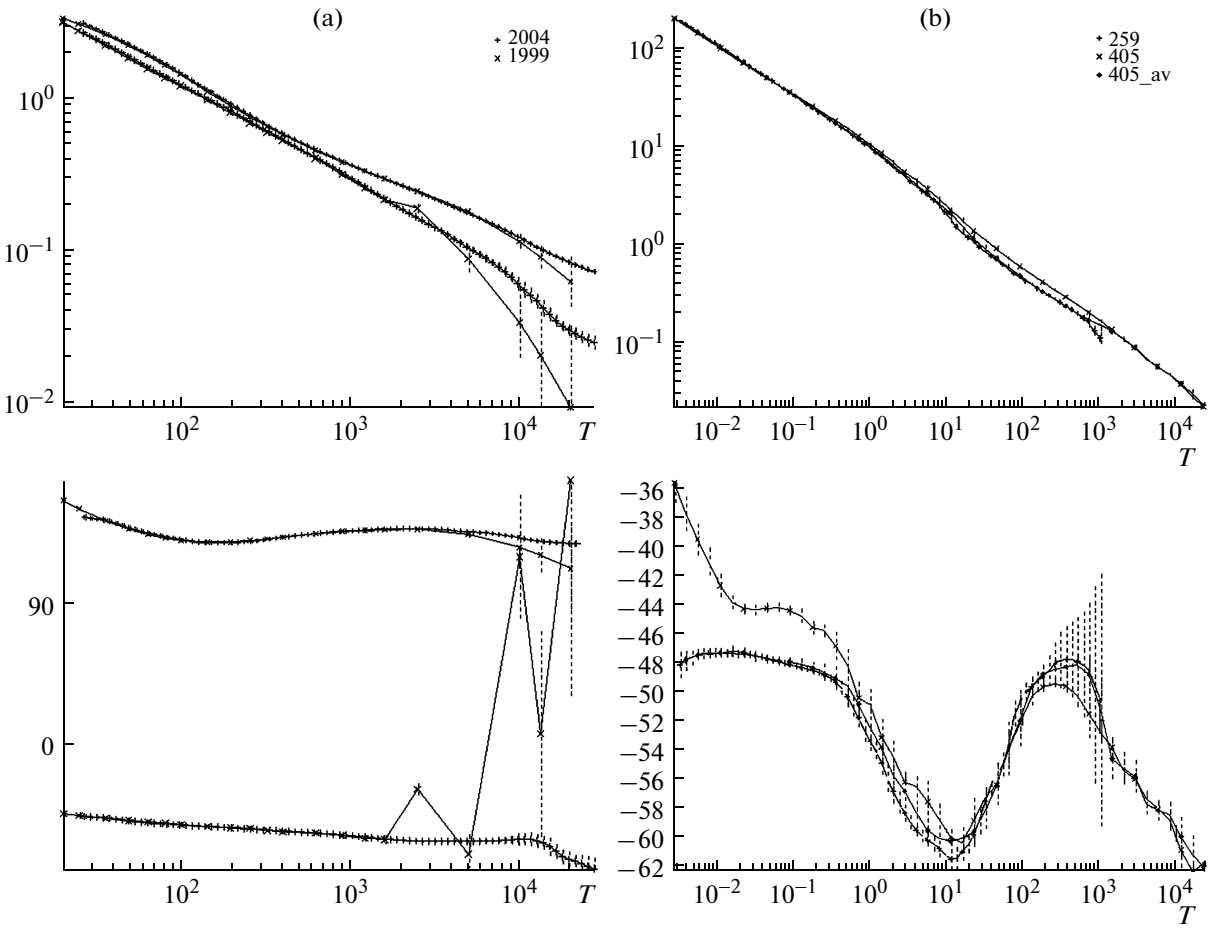

Fig. 2. Comparison (a) of the previously obtained (1999) impedance estimates at the observation point 407 of the LIMS soundings [Rybin et al., 2001] with the new estimates (2004), at the top, the amplitudes of the additional impedances Z_{xx} and Z_{yy} are presented (expressed in practical units), at the bottom, the corresponding phases are shown (expressed in degrees); (b) the amplitude estimates (at the top, expressed in practical units) and phase estimates (at the bottom, expressed in degrees) of impedance Z_{xy} at observation point 405 of the LIMS/MT24 soundings and at the close observation point 659 of the Phoenix soundings, and also the resultant estimate for observation point 405 (405_av) as a result of the robust averaging of the presented data.

on the heterogeneous grid of geotraverse observations. The transfer operators are presented for all soundings in the initial geomagnetic coordinate system with the x axis directed to the North and the y axis directed to the East. With the value of the magnetic declination on the Naryn profile less than 6°, there is no need for their recalculation in the geographical coordinate system.

The analysis of the obtained dataset makes it possible to distinguish the following two important subsets. The long-period dataset, in abbreviated form designated as **LMT**, which is based on the combined LIMS/MT24/Phoenix soundings. It contains the estimates of impedance and tipper at 19 observation points for periods 0.1–16384 s and the estimates of horizontal MV operator relative to the base at point 410 for 14 soundings (points 401–414) for periods 32–16384 s.

The reliable results of CES-2 soundings (11 observation points), MT-PIK soundings (12 observation points), LIMS/MT24/Phoenix soundings (19 observation points), and Phoenix soundings (23 observation points) composed in the limited prospecting range of periods a denser united ensemble, designated as **MT** in abbreviated form. It includes estimates of impedance within the range of periods from 0.1 to 1024 s and the tipper within the range of periods from 16 to 1024 s for 65 soundings throughout the entire length of the profile from the Lake Balkhash region up to the northern edge of the Tarim basin. The data of this ensemble essentially refine the structure of the crustal electromagnetic responses, since the step of observations in the region of the concentration of soundings decreases up to 3 to 5 km (Figs. 1, 3).

In the present analysis, the electromagnetic responses on the shortest periods (0.03–0.1 s) are not considered. They appear excessive in the course of construction of the united crustal–mantle geoelectric model along the Naryn profile, but they can be utilized subsequently for refining the structures of sedimentary cover in its separate regions.

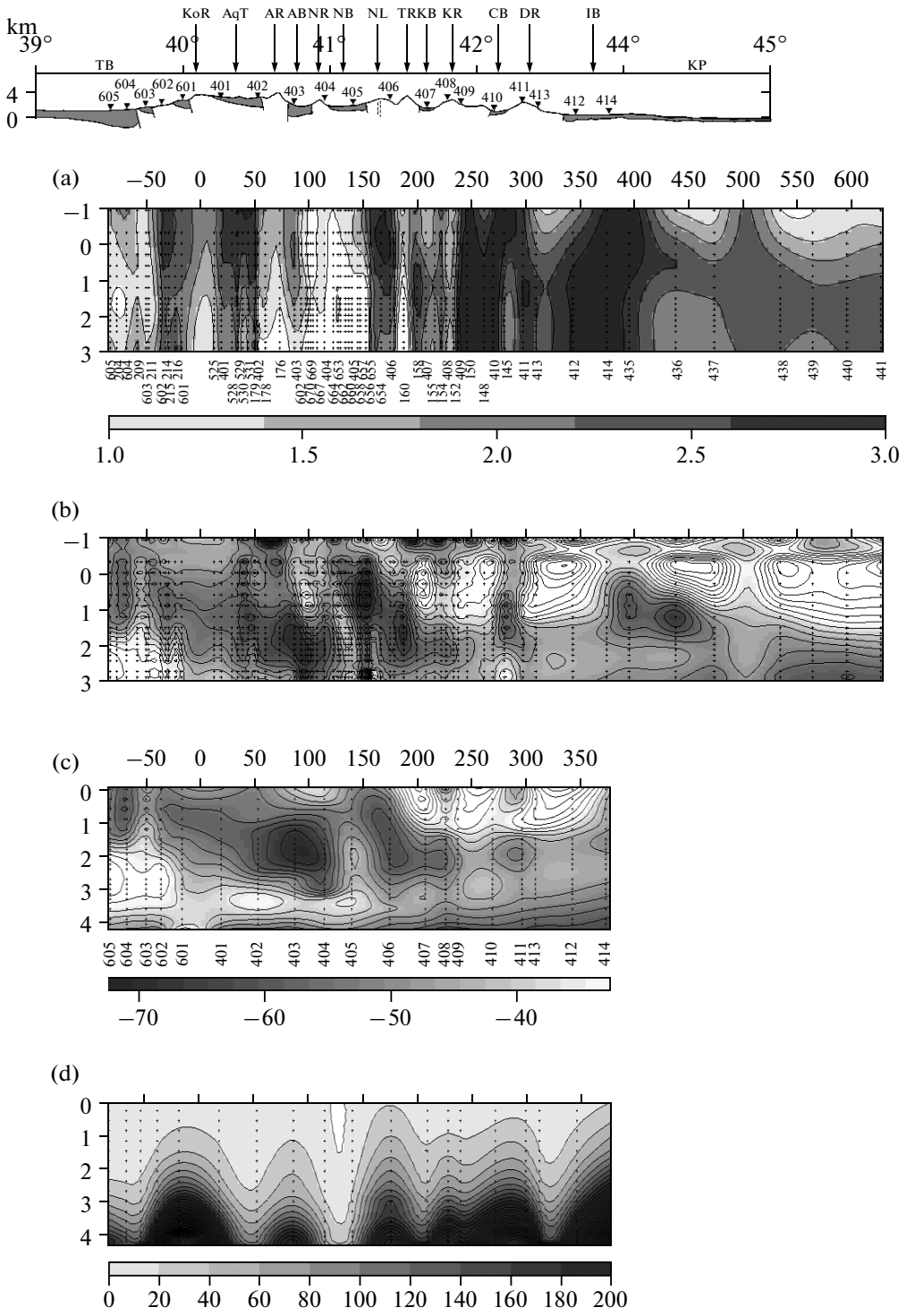

Fig. 3. Pseudosections of impedance responses for the ensemble of **MT** soundings: (a) the longitudinal apparent resistivity *Ro_Ep* (expressed in Ω m, the logarithmic scale), (b) the phase of the longitudinal impedance Arg_*Z_Ep*(expressed in degrees). Pseudosections of impedance responses for the long-period ensemble of **LMT** soundings: (c) the phase of the longitudinal impedance Arg_*Z_Ep* (expressed in degrees), (d) the estimates of the depth of penetration of electromagnetic field obtained from the effective apparent resistivity (expressed in km); the period (expressed in seconds, in the logarithmic scale) is plotted along the vertical axes; at the top, the diagram of topography and sedimentary structures: the Tarim Basin (TB), the Kokshaal Ridge (KoR), the Aqsay Basin (AT), the Atbashi Ridge (AqR), the Atbashi basin (AT), the Naryn Ridge (NR), the Naryn basin (NT), the fault zone of the Nikolaev Line (NL), the Terskey Ridge (TR), the Kochkor Basin (KT), the Kungey Ridge (KR), the Chu basin (CB), the Dzhetyzhol Ridge (DR), and the Ily Basin (IB).

The morphology of pseudosections of the MT/MV responses

Visualization of the constructed ensembles of transfer operators in the original coordinates (x is directed to the North, y is directed to the East) is highly useful, since the stretch of the prevailing geoelectric structures a priori (in accordance with the regional tectonics) is assumed to be sublatitudinal, i.e., along the y axis. The most compact form of representation of the spatial–frequency structure of the components of the transfer operators of the electromagnetic field are their pseudosections: maps with an observation profile along the horizontal axis and with the parameter of depth of penetration (the logarithm of period) along the vertical axis. The origin of coordinates on the Naryn profile is placed on the border of Kyrgyzstan and China and the profile coordinates increase from the South to the North.

The pseudosections of the apparent resistivities and impedance phases are presented in Fig. 3. The topography of the Central Tien Shan, the adjacent regions of the Kazakh and Tarim Plates, and the sedimentary structures of intermountain basins are shown in the same figure on the upper panel. The shown pseudosections reflect the wide spectrum of the anomalies of electrical conductivity in the different structural floors. The simplest estimates of the depth of penetration of soundings with respect to the skin depth for the effective apparent resistivities for the **LMT** ensemble (Fig. 3d) show that the geoelectric heterogeneities available for study lie within the range from the first hundreds of meters (the skin depth for resistivities is 10 to 100 Ω m on a period 0.1 s) up to the first hundreds of kilometers (periods higher than 7000–10000 s).

A number of striking anomalies can be correlated with the known specific features of the Central Tien Shan structure. The anomalies on the pseudosections of the apparent resistivities are tightly connected with the localization of intermountain basins and large-scale sedimentary basins. The pseudosections of the northern (the transverse *Ro_Hp*) and the eastern (the longitudinal *Ro_Ep*) components can be schematically subdivided into six regions according to the average level of resistivities. In Fig. 3a (*Ro_Ep* for **MT** ensemble), the following regions can be distinguished: the southern low-resistivity region (up to the 50 km picket), which corresponds to the sediment rock mass of the Tarim Basin wedging out northward; the high-resistivity region of the Kokshaal Ridge; the lowest-resistivity region of the Aqsay, Atbashi, and Naryn basins with the local increases in the resistivities under the Atbashi and Naryn Ridges dividing them; the high-resistivity region of the Terskey Ridge with the adjacent Kochkor basin; the region with the highest-resistivity on the profile of the Kyrgyz (Kungey) Ridge and Dzhetyzhol Ridge with their foothills; and the northern region of reduced resistivities (from the 430 km picket), caused by the growth to the North from the Ili valley of the thickness of sedimentary cover of the Kazakh Plate. The frequency dependence of the apparent resistivities, which reflects a change in the electrical resistivities with depth, is distinct only within the limits of the Kazakh Plate: here, the low resistivities of the sedimentary rocks of the cover are replaced with an increase in the period by increased values, which correspond to the basement, and further by lower values, characteristic for the conducting upper mantle. In the remaining regions of the profile, this dependence is disguised by strong static distortions.

The phase components of impedance give more meaningful information on the change in electrical resistivity with depth. The longitudinal phases are the most informative with respect to deep conductors in the course of profile interpretation. The pseudosections of the longitudinal phases for **MT** and **LMT** ensembles, respectively, are given in Figs. 3b and 3c. The negative anomaly on periods from 2–500 s (with an extremum that reaches –70° in the vicinity of the 100 s period) is most distinctly identified on them, which according to the estimates of the effective skin depth (Fig. 3d) indicates the presence of a conducting structure in the section at depths of the initial tens of kilometers. This anomaly is presented most vividly in the **MT** range (Fig. 3c): here, it is possible to trace the displacement of its extremum from periods of 2 to 5 s to 100 to 300 s in the region of the junction of the Tarim and the South Tien Shan (the subsidence of the conductor to the North?). In the short periods (the first few seconds) the influence of sedimentary basins is noticeable, which is expressed by the change of negative extrema with positive ones. The deepest valleys distort the phase response of the crustal conductor (for example, the Naryn, Chu, and Ili valleys in the neighborhood of pickets at 130 km, 260 km and 350 km, respectively).

In this stage of the analysis of impedance responses, it is expedient to consider the pseudosections of effective impedance: the simplest tensor invariant, obtained as a root from the determinant. On the pseudosections of the effective phase, the response of the conducting layer is most distinct and stable. As a whole, in all phase components in the periods of the first hundreds of seconds, a negative anomaly, connected with the conducting crustal layer, is observed. This anomaly is outlined on the larger part of the profile attenuating on the Kazakh Plate. The tendency of subsidence of the crustal conductor from the Tarim to the North is reflected in the configuration of the adjacent positive phase anomalies, caused by the structure of the upper- and lower-crustal insulators. The increased electrical conductivity of the upper mantle manifests itself in the form of negative phase anomalies on periods from 1000 to 6000 s (Fig. 3c). A significant increase in the depth of penetration of the electromagnetic field within the limits of the Kazakh Plate (Fig. 3d) in view of the high transverse resistivity of its lithosphere makes it possible on the North of the pro-

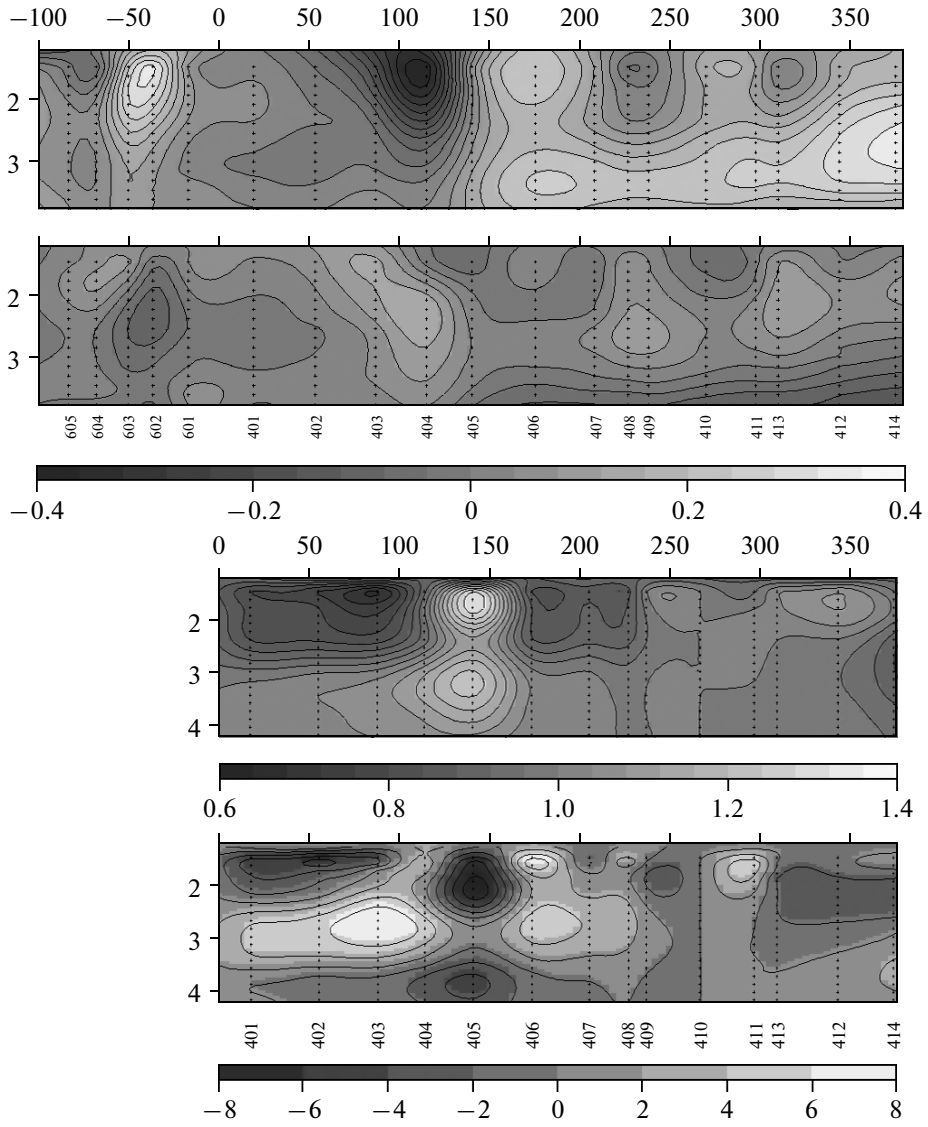

Fig. 4. Pseudosections of the components of MV responses for the long-period LIMS soundings, from top to bottom: Re_W_{zx}, Im_W_{zx}, Mod_M_{xx}, Arg_M_{xx}.

file to observe the upper-mantle effects already in periods of several hundreds of seconds.

The pseudosection of the real part of the tipper (Re_W_{zx}), presented for the **LMT** ensemble in Fig. 4, reflects well the lateral changes in the section's resistivity. The most striking effects of the alternation of the badly conducting mountainous areas and the low-resistivity fault zones (the South Tien Shan fault, points 602–601; the Atbashi–Inylchek fault, points 403–670; the Nikolaev Line, points 661–405–656; and the North Tien Shan fault, points 409–410) are deepened by the influence of sediments of the adjacent intermountain basins. The strongest and deepest contrast is noted in the Nikolaev Line zone (points 405–656). Here, the anomaly is observed on periods up to 1500 s, which makes it possible to assume the continuation of this fault zone up to a depth of several tens of kilometers. The pseudosection of the imaginary part of the tipper (Fig. 4b) reflects more distinctly the changes in the resistivity with depth.

The pseudosections of the northern (M_{xx}) component of the horizontal MV response (Figs. 4c and 4d) are characterized by the presence of a spectacular amplitude-phase anomaly in the Nikolaev Line region (points 405–657). The anomaly is decomposed into two extrema (in the periods of 50 and 2000 s for the amplitude, and 100 and 7000 s for the phase), which substantially supplements the information on the structure of this anomalous zone supplied by the data of tipper and impedance phases. Phase anomalies at

point 409 (the North Tien Shan fault?) and at points 411 and 413 (the extrema on periods from 50 to 150 s) are less distinct on the widely spaced network of observation points.

3. INVARIANT ANALYSIS OF THE TRANSFER OPERATORS

In the course of interpretation of the aggregate arrays of the MT/MV responses on the Naryn profile, the very first stage consists in the analysis of their invariant parameters to extract information on the dimensionality and the stretch of the studied geoelectric structures. Based on this information, a critical decision is made on the possibility or impossibility of a 2D inversion of the available data and, in the case of a positive decision, based on the results of invariant analysis, a 2D interpretation model is constructed [Berdichevsky and Dmitriev, 2009]. The domains of the priority search for anomalies of electrical conductivity are determined and are parametrized, the model of surrounding medium is selected, and the components of data that correspond to the accepted 2D model are extracted; the inversion algorithm and the tactics of its application are selected. Finally, the distorting 3D effects in the inverted data, their influence on the results of the profile inversion, and the possibility of its elimination are evaluated. The specific features of the construction procedure of the interpretation model are significantly determined by the data inversion algorithm. For the INV2D algorithm used by the NARYN group, these specific features are in sufficient detail presented and illustrated in the works [Varentsov, 2002; 2007a].

For determining the dimensionality and the stretch of the geoelectric structures of the Central Tien Shan, different schemes of invariant analysis of the obtained transfer operators of the electromagnetic field were investigated. However, we focused our attention on schemes that were most stable to the near-surface galvanic (static) distortions: the CBB-decomposition (Caldwell, Bibby, and Brown) of the phase impedance tensor [Caldwell et al., 2004], the Swift decomposition of the horizontal MV operator [Varentsov, 2007b], and the estimates of the dimensionality and the stretch of the structures according to the tipper data [Berdichevsky and Dmitriev, 2009]. The results of the impedance decomposition within the framework of the traditional schemes of Swift and Eggers, subjected to the essential static distortions, were examined for contrast. The details of the majority of decomposition procedures mentioned above are presented in the monograph [Berdichevsky and Dmitriev, 2009].

Determination of the Dimensionality of Geoelectric Structures

The parameter of **MT** heterogeneity N is the simplest measure of 2D/3D heterogeneity of a medium and can be obtained in the decomposition schemes of **Z** impedance that supply its principal (in some specified sense the extreme) scalar values of $Z_{\max}$ and $Z_{\min}$: $N = |Z_{\max} - Z_{\min}| / |Z_{\max} + Z_{\min}|$. Following [Berdichevsky and Dmitriev, 2009], we will consider this parameter within the framework of Eggers' decomposition, in which the principal values acquire the sense of eigenvalues. The medium is considered quasi-onedimensional with a small N ($N < 0.2$–0.3); however, this estimate is subjected to static distortions.

The asymmetry parameter $Skew_S$ in the system of Swift's decomposition is considered as the simplest parameter, an indicator of three-dimensionality of a medium: $Skew_S = |Z_{xx} + Z_{yy}| / |Z_{xy} - Z_{yx}|$. The essential three-dimensionality of the medium is manifested with the value of this parameter $Skew_S > 0.3$, but this estimate is also subjected to static distortions.

An elegant way of obtaining statically undistorted estimates of the impedance asymmetry is by the analysis of the phase impedance tensor: $\mathbf{\Phi} = [\mathrm{Re}\mathbf{Z}]^{-1} \cdot [\mathrm{Im}\mathbf{Z}]$. By definition [Caldwell et al., 2004], this operator does not depend on the frequency independent real matrix of galvanic distortions. In the CBB-decomposition of the phase tensor proposed in the paper cited above, the parameter of its angular asymmetry $Skew_{SBB} = \frac{1}{2}\arctan((\Phi_{xy} - \Phi_{yx})/(\Phi_{xx} + \Phi_{yy}))$, $\mathbf{\Phi} = \{\Phi_{ij}, i,j = x, y\}$ is introduced, which is functionally related [Caldwell et al., 2004; Berdichevsky and Dmitriev, 2009] with the dimensionless asymmetry parameter in Bahr's decomposition: $Skew_B = \sqrt{|\mathrm{Im}(Z_{xy}Z^*_{yy} + Z_{xx}Z^*_{yx})|}/|Z_{xy} - Z_{yx}|$. This last parameter, common for the Bahr and CBB (Caldwell, Bibby, and Brown) schemes, appears to be an appreciably more pragmatic diagnostic tool of the three-dimensionality of deep responses under the conditions of static distortions. The threshold of their recognition amounts to 0.2 to 0.3, which is comparable with the threshold of the $Skew_S$ parameter.

In addition to the impedance estimates of the three-dimensionality of a medium, we will also use their MV analogs. In accordance with the nature of MV data, these estimates are free from the static distortions within the range of long-period studies. For the horizontal MV operator **M**, we will use the Swift approach [Varentsov and EMTESZ-Pomerania WG, 2005; Varentsov, 2007b] and will determine the asymmetry parameter: $Skew_M = |M_{xy} - M_{yx}|/|M_{xx} + M_{yy}|$. The estimate of $Skew_M$ indicates 3D effects with a noticeably lower threshold (of the order of 0.1).

The three-dimensionality of a tipper is manifested in the misalignment of the axes of the real $\mathbf{W_{Re}}$ and imaginary $\mathbf{W_{Im}}$ induction vectors and, following [Berdichevsky and Dmitriev, 2009], can be evaluated by the parameter: $Skew^{BD}_W = |(\mathrm{Re}W_{zx}\mathrm{Im}W_{zy} - \mathrm{Re}W_{zy}\mathrm{Im}W_{zx})/(\mathrm{Re}W_{zx}\mathrm{Im}W_{zx} + \mathrm{Re}W_{zy}\mathrm{Im}W_{zy})|$, which, however, becomes unstable with small lengths of the induction

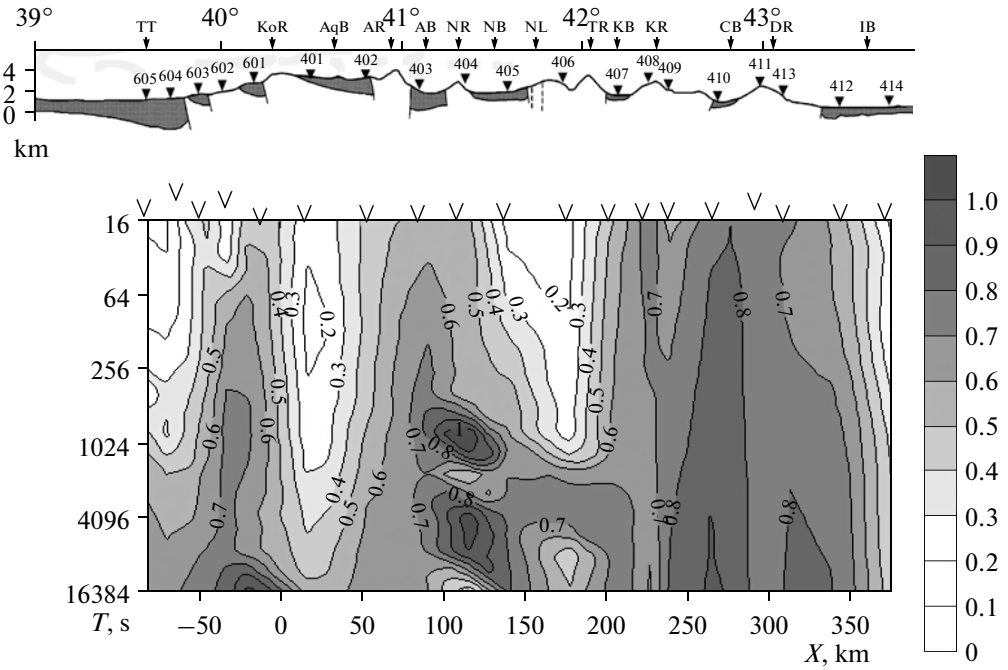

Fig. 5. Pseudosection of the impedance parameter of the medium heterogeneity N (expressed in the relative units) for the ensemble of **LMT** soundings.

vectors. For obtaining a more stable estimate of the tipper asymmetry, we will use the estimate of the θ_{max} direction of the maximum induction vector $\mathbf{W_{max}}$, determined by maximizing the amplitudes of the tipper components in the course of rotating the coordinate system, in which it is represented: $\theta_{max} = \frac{1}{2}\arctan(2\mathrm{Re}(W_{zx}W_{zy}^*)/(|W_{zx}|^2 - |W_{zy}|^2)) + n\frac{\pi}{2}$, and $n = 0, 1, 2, 3$, with the choice of a proper n. The induction vector $\mathbf{W_{max}}$ is close to the geometric sum $\mathbf{W_{Re}} + \mathbf{W_{Im}}$ and it appears as the most stable invariant for the small tippers. Now, we will determine the lengths of the perpendiculars p_{Re} and p_{Im}, built from the vertexes of the $\mathbf{W_{Re}}$ and $\mathbf{W_{Im}}$ vectors in the direction of maximum induction θ_{max}: $p_{Re} = W_{Re}|\sin(\theta_{Re} - \theta_{max})|$ and $p_{Im} = W_{Im}|\sin(\theta_{Im} - \theta_{max})|$; here, W_{Re} and W_{Im} are the lengths, and θ_{Re} and θ_{Im} are the azimuths of the corresponding vectors. The asymmetry parameter is represented by the maximum of these lengths: $Skew_W = \max(p_{Re}, p_{Im})$ and by construction is equal to zero in 1D and 2D media. At first glance, the normalization of this estimate by the value of W_{max} suggests itself, but it is not advisable for reasons of stability. The parameter of tipper asymmetry $Skew_W$ indicates three-dimensionality with a threshold of the order of 0.3.

The distribution of the heterogeneity parameter N along the Naryn profile for the **LMT** ensemble is shown in Fig. 5. The regions of gently sloping sedimentary basins (Tarim, Aqsay, Naryn, and Ili basins, where $N < 0.2$) are characterized by the relative homogeneity (quasi-one-dimensionality) of the upper part of the section. In the other regions, N is greater than 0.5, which indicates the essential 2D/3D heterogeneity of the section, or static distortions.

The pseudosections of different asymmetry estimates ($Skew_S$, $Skew_B$, $Skew_M$ and $Skew_W$) for the ensemble of **LMT** data are compared in Fig. 6. The impedance of Swift's estimate demonstrates on a significant part of the Naryn profile (especially for periods >500 s) strong 3D distortions within a wide range of periods, designated by values $Skew_S > 0.3$. In the larger part of such regions, however, the statically undistorted phase estimate $Skew_B < 0.2$ and, correspondingly, the nature of such effects is connected with near-surface distortions. According to the $Skew_B$ data, three-dimensionality is manifested within a wide range of periods only at the observation point 405 (the Nikolaev Line zone) and, to a lesser extent, at the adjacent observation point 404, and, also, at point 409 (the North Tien Shan fault). More locally (and only on periods up to 1000 s) three-dimensionality is also observed on the southern part of the profile (points 602–603, 605, and 401–402) and on the north (points 412–413). It should be noted that the three-dimensionality at the Tarim observation points can be partly explained by the increased level of uncertainties of the old evaluation of the additional impedances (Fig. 2a), since the new multisite data processing was not conducted here.

The impedance estimates of asymmetry according to the data of the **MT** ensemble confirm (on the basis of the overlapped intervals of periods) the conclusions

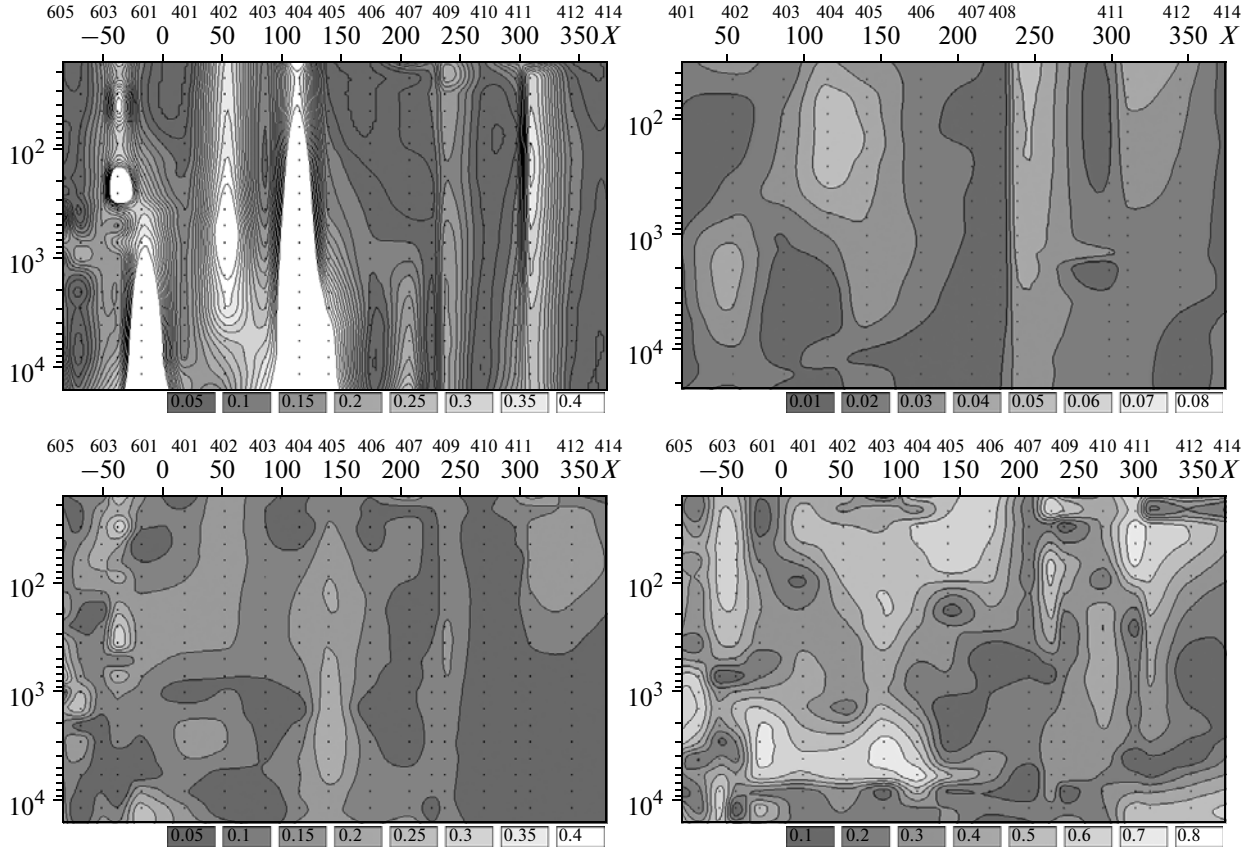

Fig. 6. Pseudosections of the distribution of the asymmetry parameters of the impedance and phase tensor (the panels on the left, from top to bottom: $Skew_S$, $Skew_B$), the horizontal magnetic tensor and tipper (the panels on the right, from top to bottom: $Skew_M$ and $Skew_W$) for the **LMT** ensemble.

made from the results of the **LMT** ensemble at points 401–402, 404–405, and 412–413, and they also identify the local regions of three-dimensionality on short periods at observation points 410–411 (the Chu valley) and at observation points 435, 436, and 440 (in periods 1–20 s).

The results of the dimensional analysis of geoelectric structures according to MV data appear noticeably simpler and, as a whole, they are well correlated with the analogous information extracted from the impedance data. The $Skew_M$ pseudosection appears to be the simplest one: there are only signs of weak three-dimensionality on it (at the level, $Skew_M = 0.06–0.08$) at the observation points 402, 404–405, 409 and 412–413. On the pseudosection of the tipper asymmetry $Skew_W$ within the long-period range, three-dimensional effects are absent on the Kazakh Plate: here, only the local effects on periods up to 1000 s at observation points 410–412 are observed. At the center of the profile, an extended region of 3D effects is observed at the observation points 401–406 up to periods 100–200 s, and also at the observation points 601–404 on the longer periods 2000–7000 s. However, these effects are not so strong in the data of the phase tensor (see the corresponding segments of the $Skew_B$ pseudosection). Apparently, the increased sensitivity of the tipper to the influence of the conducting structures, which lie beside the profile, is manifested here: a considerable increase in the longitudinal conductivity of sediments of the Naryn basin in the western direction (Fig. 8), and a possible three-dimensionality of the deep structures in the zone of intersection of the Talas–Fergana and the South Tien Shan faults (Fig. 1).

Summing up the results of the dimensionallity analysis of a geoelectric medium according to the MT and MV data, it is possible to make a conclusion about the general two-dimensionality of the crustal-mantle section, the presence of numerous near-surface 3D effects (both static effects and more complex effects, which are manifested in the impedance phases and the tipper data) and the presence of separate local 3D effects in the Earth's crust and in the upper mantle (primarily, in the neighborhood of observation points 405 and 601–403).

Determination of the Strike Direction of the Geoelectric Structures

Now, we will continue the analysis of the invariant parameters of the transfer operators of an electromagnetic field in the decomposition schemes considered in the previous section, focusing attention on the estimates of the main directions of operators that indicate in the quasi-two-dimensional case the stretch of the prevailing geoelectric structures. We will turn to the study of the statically undisturbed estimates, determined based on the MV data and the phase impedance tensor. For contrast, we will consider the statically distorted main directions of impedance in Swift's decomposition.

The main directions of impedance in the Swift scheme are orthogonal and are determined by the minimization of the amplitudes of diagonal elements in the course of rotating the coordinate system of the tensor representation. In the Swift scheme, for the horizontal MV operator only the criterion of minimization of the amplitudes of the off-diagonal elements is different. Furthermore, this scheme can be also applied to the anomalous operator $\mathbf{M_a} = \mathbf{M} - \mathbf{I}$, where $\mathbf{I}$ is the unit operator. The main directions of the phase tensor in the CBB scheme are constructed by the method of singular decomposition [Caldwell et al., 2004; Berdichevsky and Dmitriev, 2009] and are also orthogonal. In a two-dimensional medium, one of the main directions determines the direction of strike.

It is convenient to organize the visualization of the main directions and the main amplitude/phase values of impedance, as well as the horizontal MV response, for the sounding profile in the form of matrix diagrams with rows, which correspond to the observation points, and with columns, which correspond to the periods of observation. Each element of such diagrams for the decomposition schemes with the orthogonal main directions is represented by a cross, oriented along the main directions with the lengths of the cross rays, determined by the corresponding principal values: by the amplitudes or the absolute values of phases. For greater clarity, ellipses can be stretched on the constructed crosses.

The simplest amplitude diagrams appear to be of the main directions of the anomalous MV operator $\mathbf{M_a}$ with the choice of a reference point in the quasi-onedimensional normal section outside of the fundamental anomalies of electrical conductivity: ellipses are collapsed at the observation points with the normal geoelectric structure; they acquire circular form in the quasi-onedimensional regions that are different from the normal section; they are significantly stretched above the quasi-onedimensional conducting structures and are collapsed into a segment above the two-dimensional structures; finally, the moderately elongated ellipses indicate three-dimensional structures. For the diagrams of a horizontal MV response, in a number of cases, it is expedient to turn the crosses/ellipses by 90° so that the long axes clearly indicate the strike of the conducting structures.

The interpretation of analogous diagrams for the impedance amplitudes is hindered by their strong attenuation with the period and by the presence of static distortions; it is somewhat simpler for the impedance phases and it is most productive for the phase tensor. On the matrix diagrams of the induction vectors (in the Wiese convention), the stretch directions of the conducting structures are perpendicular to the direction of real vectors with a long length.

Another important form of visualization of the regular patterns of distribution of the main directions for a set of observation points and the periods of observation are sector histograms, which statistically indicate the strike dominants and characterize their stability. Extensive experience of construction and visualization of the main directions of MT/MV responses is accumulated in the course of data analysis of synchronous EMTESZ-Pomerania soundings and is presented in the works [Varentsov et al., 2005; Varentsov and EMTESZ-Pomerania WG, 2005; Ernst et al., 2008].

In Fig. 7, along the Naryn profile, for the **LMT** data set, the matrix cross diagrams of the main directions of impedance (Swift's scheme), the phase impedance tensor (the CBB scheme), and the anomalous horizontal MV response are compared with the diagram of induction vectors. The diagrams for the phase tensor demonstrate the most regular structure. The long-period data (>1000 s) are characterized by a very stable orientation of the main directions along and across the profile. On the Kazakh Plate, such orientation is outlined already from the period of 100 s. This regularity agrees well with the latitudinal strike of the structures of the Central Tien Shan. Individual exceptions in the long-period range are observed at observation point 405, with essential fundamental three-dimensionality (Fig. 6) and at observation point 402 (up to the period of 4000 s). In the limits of the Tarim segment of the profile, the regular turning of the long-period diagrams approximately by 20° eastward is observed. In the central and Tarim segments, on the periods 16–512 s, several local anomalies of the crustal depth are manifested in the main directions and in the phases. The diagrams of the main directions of impedances and Swift's phases also manifest the regular patterns noted above, but with a large scatter and with a large number of explicit distortions.

The main directions and amplitudes of the horizontal MV operator $\mathbf{M_a}$ (determined relative to the base at observation point 410) demonstrate the fundamental two-dimensional character of this response with the sublongitudinal strike estimate on the larger part of the profile within the long-period range (>1000 s). On the northern part of the profile (at observation points 406–412), in this range, the quasi-onedimensional structure of the response is observed (which confirms the rationality of the choice of the base at observation point 410); however, in periods up to 1000 s, the two-dimensional structure of

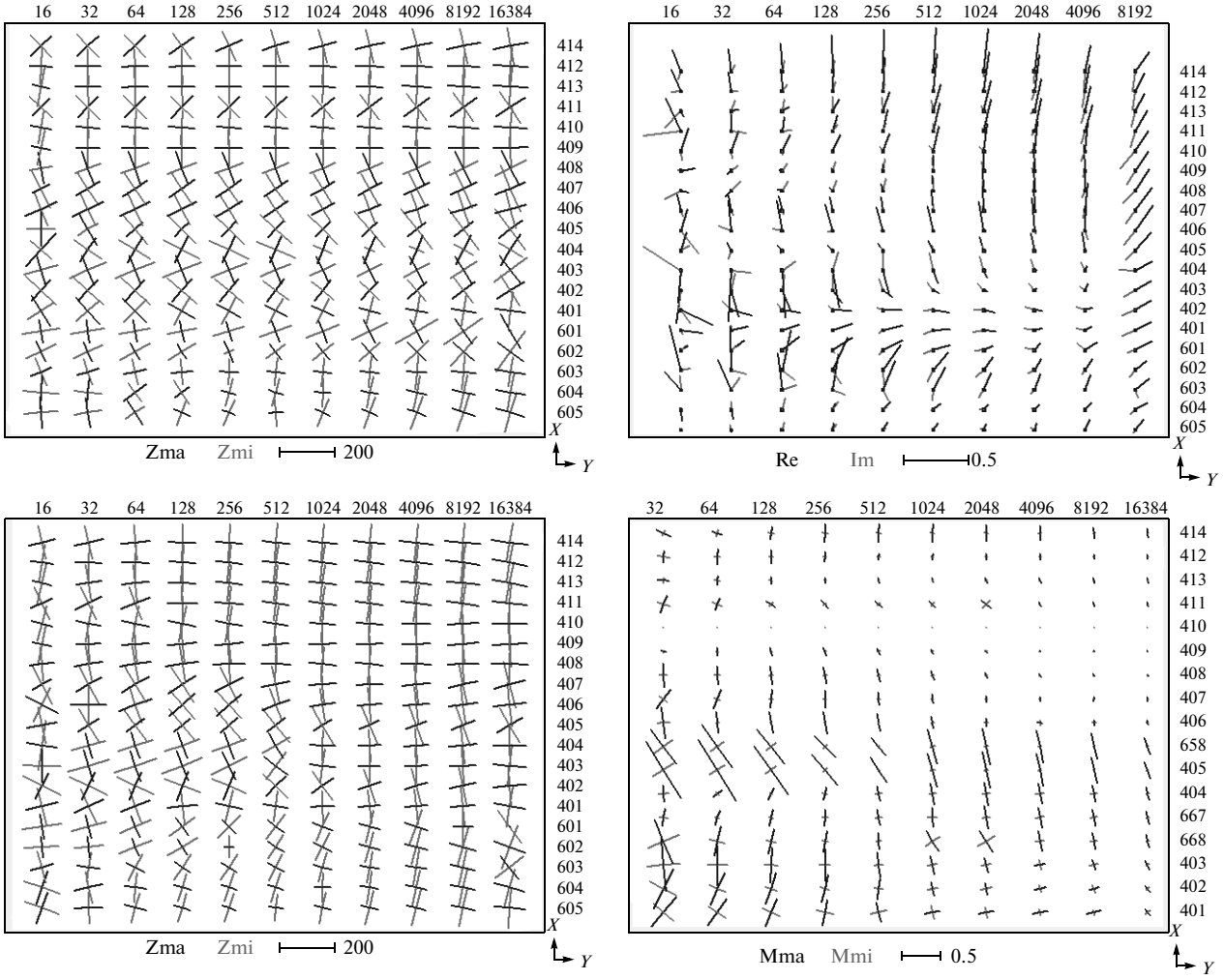

Fig. 7. Diagrams of the principal values and directions of the MT/MV responses for the ensemble of **LMT** soundings: on the left, from top to bottom, the impedance phase responses in the Swift and CBB schemes; on the right at the top, the induction vectors (Re and Im); on the right at the bottom, the amplitude responses of the horizontal MV operator $\mathbf{M_a}$; the periods (expressed in seconds) are plotted along the horizontal axes of the panels, the points of the sounding from the south (at the bottom) to the north (at the top) are plotted along the vertical axes; and the system of coordinates of soundings is shown at the bottom left angle of the panels.

the sublatitudinal stretch is also observed here. The most striking long-period 2D anomalies are observed in the central zone at observation points 658–668; moreover, at observation points 658 and 405, in the shorter periods, anomalies are increased, but change their orientation and become three-dimensional. In the South Tien Shan segment of the profile (observation points 401–403), the moderate two-dimensional character of the sublatitudinal stretch is outlined in the periods of hundreds of seconds. For the long periods, the maximum rays of the crosses become shorter and they are turned across the profile.

The positive anomalies of the maximum amplitude of the horizontal MV response are arranged directly above the regions of the increased electrical conductivity. In the axial parts of such regions, the real induction vectors, on the contrary, have the minimum (close to zero) length and further along the profile, already outside these regions, they reach their maximum length, being oriented away the source. The combined analysis of the diagrams of horizontal MV responses and induction vectors confirms that the most striking anomaly of electrical conductivity is located between observation points 658–668 at depths, which correspond to periods from tens to 4000 s. In this case, the northern boundary of this zone is very distinct between observation points 658 and 406, while its southern boundary (within the limits of points 401–403) is badly determined in connection with the different manifestation of anomalous effects on different periods and the probable interference of the effects of a different depth of penetration. The same data on the smaller periods indicate the anomaly of electrical conductivity on the very southern end of the profile.

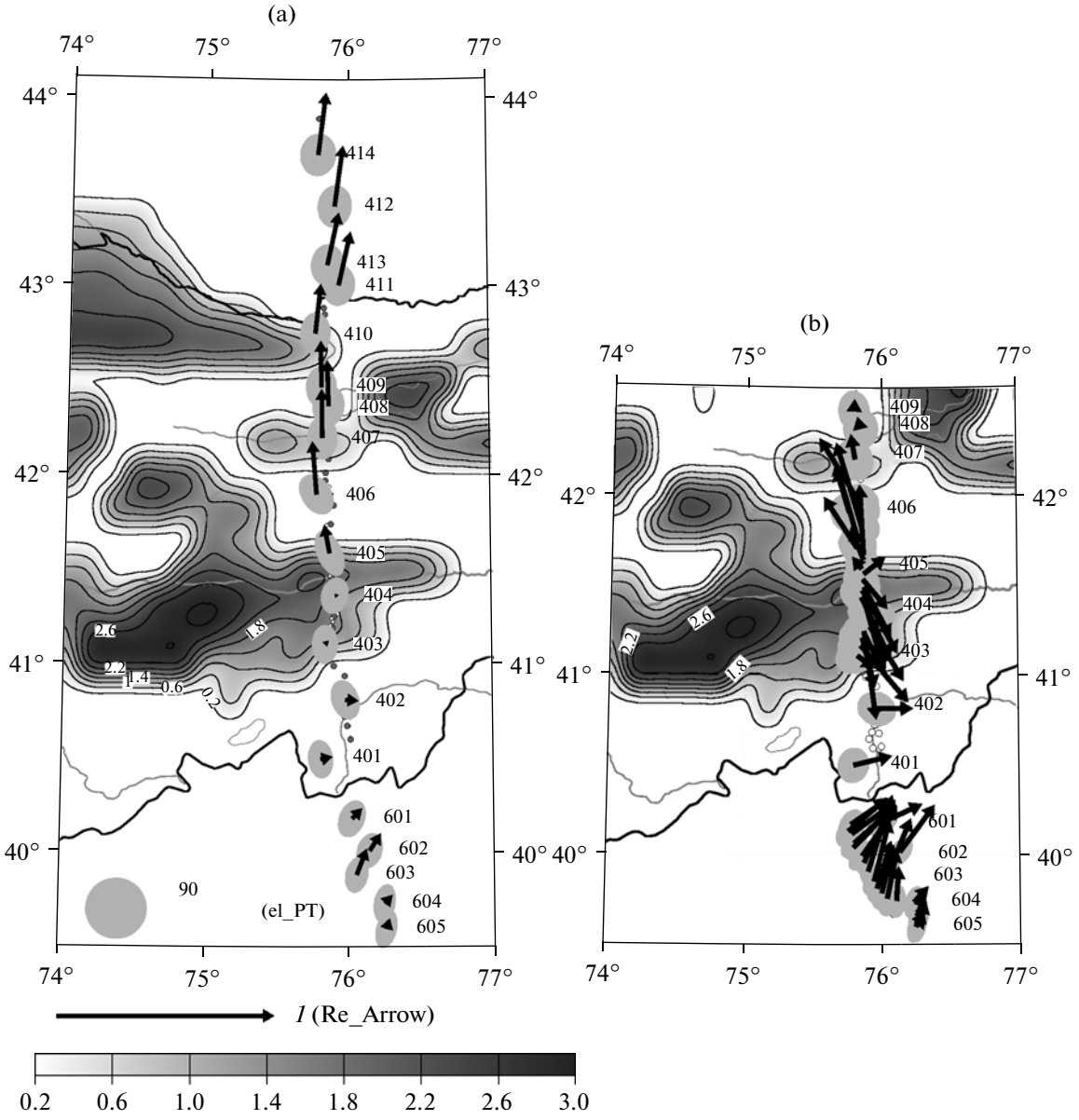

Fig. 8. Ellipses of the extreme values of the phase impedance tensor and the induction vectors (Re) (a) for a period of 2048 s along the whole length of the profile, (b) for a period of 256 s in the Nikolaev Line zone against the background of the map of the total longitudinal conductance of the sedimentary cover of the Central Tien Shan [Melnikova, 1991]; the scale of the induction vectors is assigned by the pointer of a unit length; the scale of the values of the phase tensor is assigned by a circle of radius 90°; the integral conductivity is given in S (in the logarithmic scale).

In the South Tien Shan region and its junction with the Tarim, the region of the appreciable 3D distortions of the tipper data on the periods 2000–7000 s is revealed. Among all of the considered responses, the induction vectors most vividly react on the three-dimensional sedimentary structures located westward from the profile (Fig. 8) and are turned in the opposite eastern direction. Further to the south, the induction vectors begin to reflect the influence of the Tarim structures and they acquire the stable north-northeast (NNE) orientation, as well as the principal axes of the phase tensor. Thus, it is possible to conclude that on the Naryn geotraverse, the region of sufficiently strong 3D distortions of the tipper is present; however, it occupies no more than a tenth of the profile (Fig. 1). The induction vectors within the range 16–7500 s on the entire profile, with the exception of the region indicated above, confirm, together with the data of the phase impedance tensor and the anomalous horizontal MV response, the sublatitudinal stretch of the main

geoelectric structures of the Central Tien Shan. However, in periods longer than two hours, the strong effect of the source heterogeneity appears in them (Fig. 7), which disguises the responses of deep geoelectric heterogeneities.

The analysis of the area distributions of the main directions of electromagnetic responses on a number of characteristic periods makes obvious the fact that their behavior within the limits of the Central Tien Shan is rather distinctly controlled by the boundaries of the geotectonic provinces (Fig. 8). The region of Caledonides of the North Tien Shan (points 414–406) is characterized by the submeridional direction of the real induction vectors, the minimal principal axes of phase, and the maximal principal axes of the anomalous horizontal MV tensor. The region of Hercynian Central Tien Shan (the Naryn segment, points 405–403) is characterized by the noticeable deviations of the principal directions considered westward (after inversion between points 404 and 403, the induction vectors in the south of this segment deviate eastward). Here, the principal directions of the phase tensor, which loose the submeridional and sublatitudinal orientation only at point 405, are most stable.

The consideration of the principal directions in the background of the map of integral electrical conductivity of the sedimentary cover of the Kyrgyz Tien Shan [Melnikov, 1991] explains the specific aspects of their anomalous behavior, in particular, on such an important segment of the profile as the Naryn segment. Figure 8 shows that for the data of the **MT** ensemble, the local anomalies in the behavior of the principle directions of the phase tensor and induction vectors are to a considerable extent caused by the sediment distribution in the two adjacent intermountain basins: the deeper Naryn basin and the smaller in size Atbashi basin, separated by a narrow mountain range (Fig. 1). The valleys intersect the Naryn profile in the sublatitudinal direction; however, the isolines of integral conductivity in the region of the most developed sedimentary cover located westward are stretched in the northeast-east (NEE) direction, which is orthogonal to the direction of the induction vectors in this segment and which is very close to the maximum amplitude direction of the horizontal MV tensor in the neighborhood of point 405.

The data analysis of the **MT** ensemble confirms the fundamental detailed elaboration of the conclusions made based on the **LMT** ensemble. The cross diagrams of the phase tensor and the induction vectors for periods 16–1024 s are shown in Fig. 9. The new features of the behavior of the invariants of the phase tensor and induction vectors are revealed in the segment of the detailed elaboration of the fault zone of the Nikolaev Line. In periods 64–1024 s, for observation points 404–651, the turning of the principal axes of the ellipses of the phase tensor by 30° westward, and at

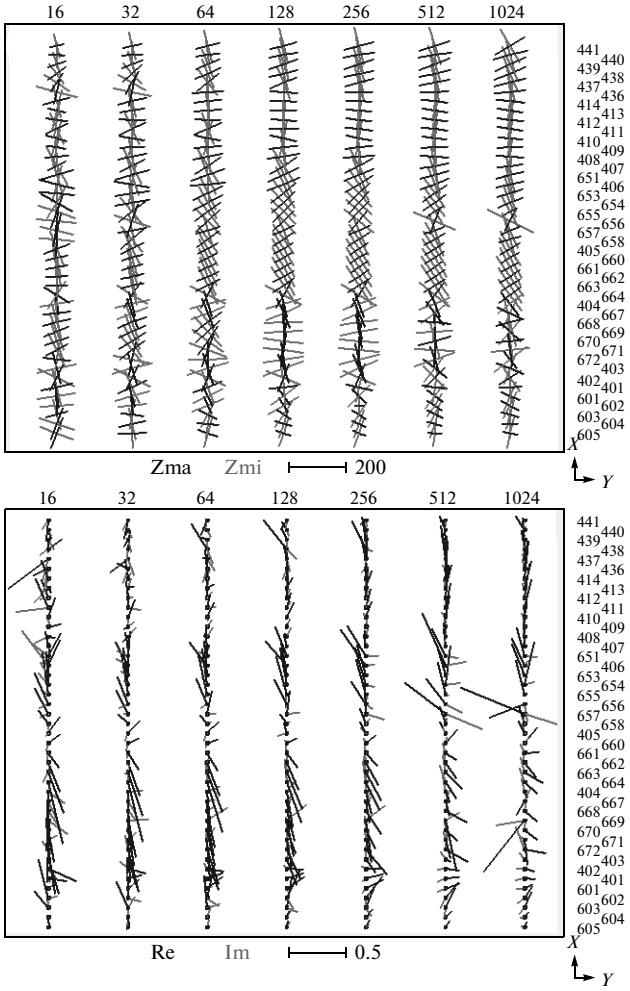

Fig. 9. Diagrams of the principal values and directions of phase tensor responses (the CBB scheme, at the top) and the induction vectors (Re and Im, at the bottom) for the **MT** ensemble; the axes are similar to those presented in Fig. 7.

observation points 672–404, a similar turning in shorter periods (2–64 s), are outlined. The induction vectors at these points are also turned in the appropriate directions; moreover, the inversion of their directions and, correspondingly, the axis of the anomaly of electrical conductivity are determined at observation points 660 and 661, located 20 km southward and marked according to the geological data as the Nikolaev Line. Figure 9 also makes it possible to trace how, with an increase in the period, the morphology of electromagnetic responses from the conductivity distribution of the sedimentary cover in the neighborhood of this complex segment of the profile is changed. The maximum influence of sediments is observed on the sufficiently long periods 128–256 s.

According to the results of the analysis carried out, it is possible to conclude that the predominant sublat-

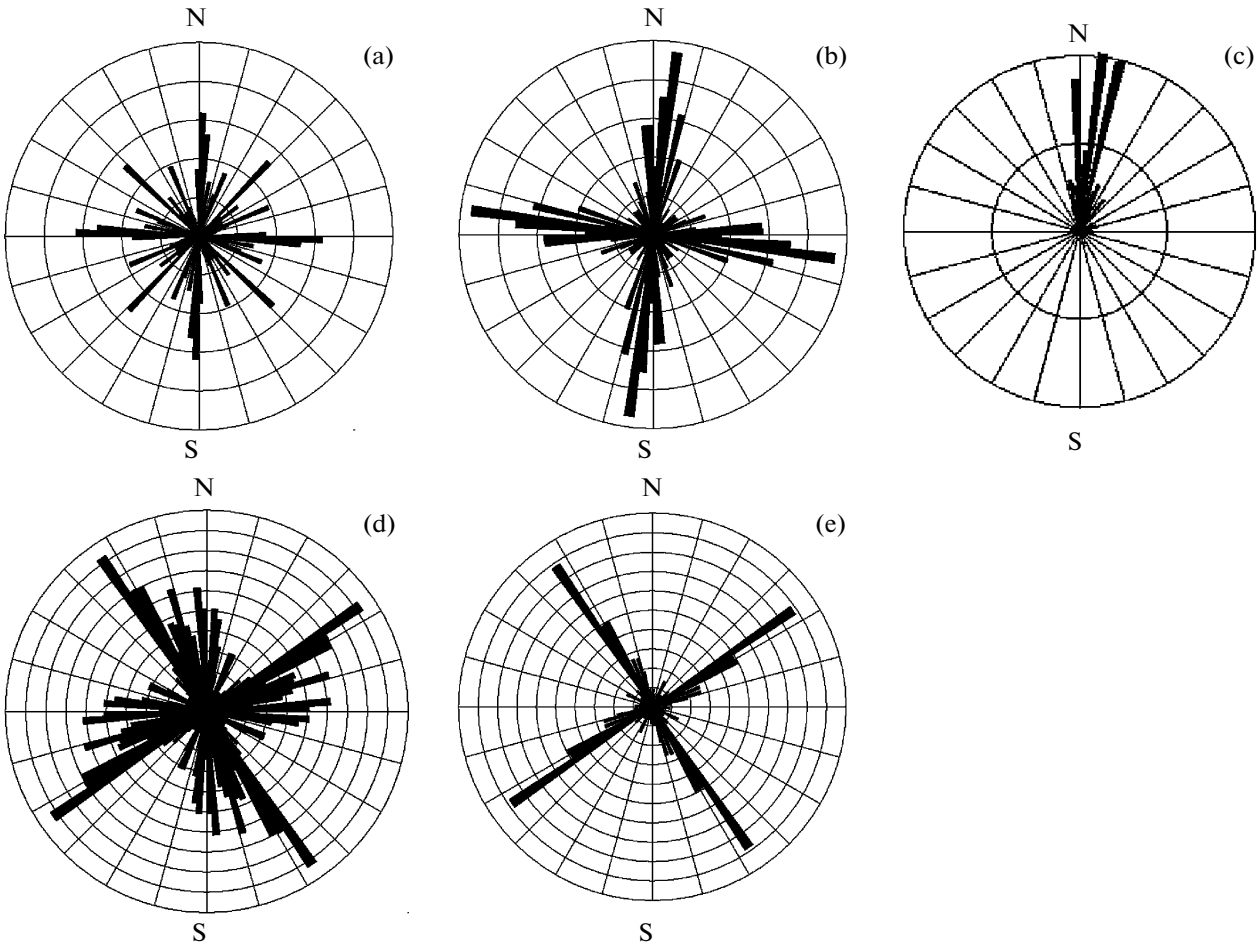

Fig. 10. Sector histograms of the principle directions of the MT/MV responses, the estimates for all 19 sites of **LMT** ensemble are shown in the upper row for periods 256–4098 s: (a) the principle directions of impedance according to Swift's scheme, (b) the principle directions of the phase tensor of impedance according to the CBB scheme, (c) the induction vectors (Re); the principle directions of phase tensor according to the CBB scheme are presented in the bottom row for periods 64–1024 s, (d) for all 65 points of the **MT** ensemble, (e) for its subset of 27 points of the Phoenix and LIMS soundings in the Nikolaev Line zone.

itudinal direction of the geotectonic structures of the Central Tien Shan is reflected in the orientation of the principle directions of the transfer operators of the **MT** and **LMT** ensembles along the Naryn profile. This correspondence is held most strictly within the interval of periods 512–4098 s. In the shorter periods, in different degrees for different responses and segments of the profile, the effects of near-surface and upper-crustal 3D heterogeneities are present, which contribute to the noticeable disturbances in the orientation of principle directions. The principle directions of the phase tensor and horizontal MV response, oriented in accordance with the regional tectonics up to the longest periods of evaluation in the **LMT** ensemble, are most stable. In contrast to the tipper data, they do not manifest essential dependence on the effects of the source's heterogeneity for periods above 2 hours. In the segment of the profile that intersects the Naryn basin, the regular and consistent turn in all transfer operators of the azimuths of their principal directions by 30° westward, caused by the configuration of the sedimentary basin, is revealed.

These conclusions are statistically confirmed with the aid of the sector histograms of the distributions of the principal directions. They are presented in Fig. 10 separately for the **LMT** and **MT** ensembles. In the **LMT** ensemble, the extremum of the azimuths of the real induction vectors and one of the extrema of the principle directions of the phase tensor coincide, amounting to ~7° (in the NNE direction), which determines the strike azimuth of the prevailing structures ~–83° (in the NWW direction). The histogram of the estimates of the principle directions of impedance according to Swift's scheme clearly shows the extent to which their scatter under the influence of the static near-surface distortions increases.

In the bottom row of Fig. 10, the histograms of estimates of the principal directions of the phase tensor in the range 16–1024 s are compared in two variants: for

all 65 points of the profile included in the **MT** ensemble, and for the subset of 27 detailed soundings on the 80-km segment of the Nikolaev Line zone. In the former, two clusters of directions are revealed: the submeridional and the northwestern (~–30°) directions, and in the latter only one prevailing direction remains (~–30°). The former is orthogonal to the regional stretch of the structures, and the latter is orthogonal to the stretch of the Naryn basin.

The results obtained substantiate the possibility of a 2D interpretation of the accumulated data, indicate the ways of selecting their most informative components, and evaluate the degree of their distortion by the 3D effects. The next papers of this cycle are concerned with the different approaches of 2D interpretation of the MT/MV data on the Naryn profile within the context of the overall inversion scheme [Varentsov, 2002; 2007a]. An important specific feature of this scheme is the minimization of the functionals of discrepancy in the robust Huber norm, which makes it possible to constrain the influence of the local data distortions, including the 3D distortions, considered above in detail. In this scheme, there is an explicit way of suppressing such distortions by increasing the data's errors in the inversion procedure proportionally both to the asymmetry parameter corresponding to them (the explicit three-dimensionality of a medium) and to the deviation of the corresponding estimate of the stretch from the strike from the parallel to the profile direction (two-dimensionality, which does not correspond to the profile position, or three-dimensionality).

CONCLUSIONS

In the paper considered, an a modern procedure of processing and analysis of the MT/MV data, adapted to the high-mountain conditions of the Tien Shan is presented. This procedure was tested in detail on the materials of electromagnetic soundings on the Naryn profile. The use of the new noise-suppression mRRMC technology [Varentsov, 2007b] for estimating the MT/MV transfer functions on synchronous soundings and the extension of all reliable data obtained on the profile in the past two decades have made it possible to prepare the good quality data within the range of periods from 0.1 to 16000 s for subsequent interpretation of the multicomponent ensemble. This ensemble includes the estimates of the local (impedance, tipper) and the two-point synchronous (horizontal MV response) transfer operators and provides the resolution of the sedimentary, crustal, and upper-mantle structures.

For determining the parameters of dimensionality and strike directions of the prevailing deep geoelectric structures, schemes that are robust to the near-surface galvanic distortions of invariant analysis of the transfer operators are selected [Caldwell et al., 2004; Berdichevsky and Dmitriev, 2009; Varentsov, 2007b]. As a whole, they revealed the regional-two-dimensional character of electromagnetic responses on the Naryn profile and indicated the possibility in principle of interpreting the accumulated data within the framework of 2D model concepts. However, it should be emphasized that in this study special attention was turned to the sophisticated quantitative analysis of the invariant MT/MV parameters, which give evidence of the dimensionality and the stretch of geoelectric structures, for the purpose of further accounting for the degree of 3D data distortion in the procedures of 2D interpretations.

The pseudosections of the MT/MV responses along the studied geotraverse abound with striking anomalies within different ranges of periods. Two regions of substantially two-dimensional responses from the sublatitudinal crustal and upper-mantle structures, which are related to the Kazakh Plate and the North Tien Shan (points 414–406), are distinctly identified; the Central Tien Shan region (point 405) is distinguished by the local 3D crustal anomaly in the fault zone of the Nikolaev Line; the South Tien Shan region (points 402–601) is subjected to the influence of remote 3D structures, which are located outside of the profile; and the border region of the Tarim Basin (points 602–605) with a quasi-two-dimensional character is not completely orthogonal to the profile's direction. In the tipper data in periods larger than 8000 s, the effects of the heterogeneous external source prevail; thus, in the course of interpretation, these data should be used for the period till 8192 s.

The most fundamental 3D distortions of data have a near-surface nature and are connected with the structures of mountain topography and sediments of intermountain basins. These near-surface effects appear essentially in periods up to the first hundreds of seconds. The analysis of the data set in the detailed Naryn segment of the profile (Fig. 8b) showed that the anomalous effects within this range of periods are determined, to a considerable degree, by the spatial structure of the Naryn and Atbashi basins. The topographic effects appear also in periods of thousands of seconds, introducing noticeable distortions in the responses of the crustal–mantle structures (for example, in horizontal magnetic tensor responce[Sokolova and Varentsov, 2009]). A detailed account in the interpretation model of a priori concepts concerning the topography and the sedimentary structures will contribute to a more reliable resolution of the deep geoelectric structures. The additional weighting of the data being interpreted taking into account their 3D distortions will also facilitate this [Sokolova et al., 2007; 2008]. The strategy and tactics of 2D inversions of the prepared data is subject to refinement with the use of imitation data [Sokolova and Varentsov, 2009].

At present, the geoelectric structure of active orogens is studied increasingly extensively in many regions of the world. In this case, the soundings, as a rule, are conducted within the framework of the pragmatic profile mode. This makes it possible to assume that the presented experience of the Central Tien Shan study and the developed methodic approaches will be useful in planning and conducting similar new studies.

ACKNOWLEDGMENTS

This work was supported by the Russian Foundation for Basic Research, project nos. 08-05-00875a and 07-05-92124a.

REFERENCES

1. M. N. Berdichevsky and V. I. Dmitriev, *Models and Methods of Magnetotellurics* (Nauchnyi Mir, Moscow, 2009) pp. 1–679.
2. M. N. Berdichevsky, Iv. M. Varentsov, N. S. Golubtsova, P. Yu. Pushkarev, A. K. Rybin, and E. Yu. Sokolova, "The Geoelectric Section of the Central Tien Shan: Sequential Inversion of the Data of Magnetovariation and Magnetotelluric Soundings along the Naryn Profile," Fiz. Zemli (2010) (in press).
3. M. N. Berdichevsky and M. S. Zhdanov, *Interpretation of the Anomalies of the Variable Electromagnetic Field of the Earth* (Nedra, Moscow, 1981) pp. 1–327.
4. R. A. Bielinski, S. K. Park, A. Rybin, V. Batalev, S. Jun, and Ñ. Sears, "Lithospheric Heterogeneity in the Kyrgyz Tien Shan Imaged by Magnetotelluric Studies," Geophysical Research Letters **30** (15), 1806, doi:10.1029/ 2003GL017455 (2003).
5. G. T. Caldwell, H. M. Bibby, and C. Brown, "The Magnetotelluric Phase Tensor," Geophys. J. Int. **158**, 457–469 (2004).
6. A. D. Chave, D. J. Thomson, and M. E. Ander, "On the Robust Estimation of Power Spectra, Coherences, and Transfer Functions," J. Geophys. Res. **92** (B1), 633–648 (1987).
7. *Contemporary Geodynamics of the Regions of Intracontinental Orogenesis (the Central Asia)*, Ed. by N. P. Laverov et al., (Nauchnyi Mir, Moscow, 2005) pp. 1–400.
8. D. G. Egbert, "Processing and Interpretation of EM Induction Array Data," Surv. Geophys. **23** 207–249 (2002).
9. T. Ernst, H. Brasse, V. Cerv, N. Hoffmann, J. Jankowski, W. Lozwiak, A. Kreutzmann, A. Neska, N. Palshin, L. B. Pedersen, M. Smirnov, E. Sokolova, and Iv.Varentsov, "Electromagnetic Images of the Deep Structure of the Trans-European Suture Zone beneath Polish Pomerania," Geophys. Res. Let. **35**, 15307, doi:10.1029/ 2008GL034610 (2008).
10. T. D. Gamble, W. M. Goubau, and J. Clarke, "Magnetotellurics with a Remote Magnetic Reference," Geophysics **44**, 53–68 (1979).
11. P. A. Melnikova, "The Maps of the Total Longitudinal Conductance of the Mesocenozoic Deposits of the Intermountain Basins of Kyrgyzia," in *The Structure of the Tien Shan Lithosphere*, Ed. by F. N. Yudakhin (Ilim, Bishkek, 1991) pp. 100–111.
12. A. K. Rybin, V. Yu. Batalev, E. Yu. Bataleva, and V. Yu. Matyukov, "Magnetotelluric Evidences of the Deep Geodynamic Conditions in the Junction Zone of the South Tien Shan and the Tarim," Zapiski Gornogo Instituta, **183** 272–276 (2008).
13. A. K. Rybin, V. Yu. Batalev, P. V. Ilichev, and G. G. Shchelochkov, "Magnetotelluric and Magnetovariation Studies of the Kyrgyz Tien Shan," Geol. Geofiz. **42** (10), 1566–1173 (2001).
14. E. Sokolova, M. Berdichevsky, Iv. Varentsov, A. Rybin, N. Baglaenko, V. Batalev, N. Golubtsova, V. Matukov, and P. Pushkarev, "Advanced Methods for Joint MT/MV Profile Studies of Active Orogens: The Experience from the Central Tien Shan," in *Protokoll uber das 22 Kolloquium "Elektromagnetische Tiefenforschung"* Ed. by O. Ritter and H. Brasse (Dtsch. Geophys. Ges., Potsdam, Germany, 2007) pp. 132–141.
15. E. Sokolova, M. Berdichevsky, Iv. Varentsov, A. Rybin, N. Golubtsova, P. Pushkarev, N. Baglaenko, and V. Matukov, "Geoelctrical Cross-Section of Central Tien Shan and Geodynamic Implications," in *19th Int. Workshop on EM Induction in the Earth (Extended Abstracts. V. 1)* (Beijing, China, 2008) pp. 203–208.
16. E. Yu. Sokolova and Iv. M. Varentsov, "Study of the Topography Effects in the MT/MV Profile Interpretation in High Mountain Regions," in *The China Int. Geo-EM Workshop (Extended Abstracts)* (Guilin, China, 2009) pp. 11–14.
17. E. Yu. Sokolova, Iv. M. Varntsov, and EMTESZ-Pomerania WG, "The RRMC Technique Fights Highly Coherent EM Noise," in *Protokoll uber das 21 Kolloquium "Elektromagnetische Tiefenforschung*", Ed. by O. Ritter and H. Brasse (Dtsch. Geophys. Ges., Potsdam, Germany, 2005) pp. 124–136.
18. Yu. A. Trapeznikov, E. V. Andreeva, V. Yu. Batalev, M. N. Berdichevsky, L. L. Vanyan, A. M. Volykhin, N. S. Golubtsova, and A. K. Rybin, "Magnetotelluric Soundings in the Kyrgyz Tien Shan Mountains," Fiz. Zemli, No. 1, 3–20 (1997).
19. L. L. Vanyan, M. N. Berdichevsky, P. Yu. Pushkarev, and P. V. Romanyuk, "The Geoelectric Model of the Cascadia Subduction Zone," Fiz. Zemli, No. 10, 23–53 (2002).
20. Iv. M. Varentsov, "Arrays of Simultaneous Electromagnetic Soundings: Design, Data Processing and Analysis," in *Electromagnetic Sounding of the Earth's Interior. Methods in Geochemistry and Geophysics*, Ed. by V. V. Spichak (Elsevier, 2007b) pp. 263–277.
21. Iv. M. Varentsov, "Joint Robust Inversion of Magnetotelluric and Magnetovariational Data," in *Electromagnetic Sounding of the Earth's Interior. Methods in Geochemistry and Geophysics*, Ed. by V. V. Spichak (Elsevier, 2007a) pp. 189–222.
22. I. M. Varentsov, "General Approach to the Solution of Inverse Problems of Magnetotellurics in the Piecewise-Continuous Media," Fiz. Zemli, No. 11, 11–33 (2002).
23. Iv. M. Varentsov and EMTESZ-Pomerania WG, "Method of Horizontal Magnetovariational Sounding: Techniques and Application in the EMTESZ-Pomerania Project," in *Protokoll uber das 21 Kolloquium "Elektromagnetische Tiefenforschung"* Ed. by O. Ritter and H. Brasse (Dtsch. Geophys. Ges., Potsdam, Germany, 2005) pp. 111–123.

24. Iv. M. Varentsov, N. G. Golubev, V. V. Gordienko, and E. Yu. Sokolova, "The Study of Deep Geoelectric Structure along the Lincoln Line Profile (EMSLAB Experiment)," Fiz. Zemli, No. 4, 124–144 (1996).

25. Iv. M. Varentsov, E. Yu. Sokolova, and the Working Group of the BEAR project, "Diagnostics and Suppression of the Auroral Distortions of the Transfer Operators of the Electromagnetic Field in the BEAR Experiment," Fiz. Zemli, No. 4, 21–48 (2003).

26. Iv. M. Varentsov, E. Yu. Sokolova, and EMTESZ WG, "The Magnetic Control Approach for the Reliable Estimation of Transfer Functions in the EMTESZ-Pomerania Project," Publ. Inst. Geophys. Pol. Acad. Sci. **C-95** (386), 68–79 (2005).

27. Iv. M. Varentsov, E. Yu. Sokolova, E. R. Martanus, and EMTESZ-Pomerania WG, "Array View on EM Transfer Functions in the EMTESZ-Pomerania Project. Study of Geological Structures Containing Well-Conductive Complexes in Poland," Publ. Inst. Geoph., Pol. Acad. Sci. **C-95** (386), 107–121 (2005).

28. Iv. M. Varentsov, E. Yu. Sokolova, E. R. Martanus, and K. V. Nalivaiko, and the Working Group of the BEAR project, "Methodology of the Construction of Transfer Operators of the Electromagnetic Field for the Array of Synchronous BEAR Soundings," Fiz. Zemli, No. 2, 30–61 (2003).